Spectral and dynamical properties of multiexcitons in semiconductor nanorods

Krishan Kumar[1] and Maria Wächtler [2]**

[1]Department Functional Interfaces, Leibniz Institute of Photonic Technology Jena, Albert-Einstein-Straße 9, 07745 Jena, Germany

[2]Chemistry Department and State Research Center OPTIMAS, RPTU Kaiserslautern-Landau, Erwin-Schrödinger-Str. 52, 67663 Kaiserslautern

*Correspondence: kumar.krishan@leibniz-ipht.de, maria.waechtler@chem.rptu.de

KEYWORDS. Multiexcitons, Auger recombination, Surface exciton, Nanorods, Markov Chain Monte Carlo, Transient absorption.

ABSTRACT. Understanding multiple charge carrier relaxation dynamics in semiconductor nanocrystals is crucial for utilizing their full potential, as it allows to guide the design of optimized structures. Multiple excitons dynamics often are characterized via the observation of additional fast exponential kinetics at band edge in transient absorption spectroscopy data with increasing excitation intensities. However, these investigations are complicated by the formation of surface localized excitons which also introduce additional fast decay components which could falsely be interpreted as multiexciton kinetics in semiconductor nanocrystals. Another challenge presents the generation of a distribution of species in dependence of the excitation intensity not only including single and double excited systems, but even higher-order multiple excitons. In this study we used intensity dependent transient absorption spectroscopy with broadband probing spanning the whole visible range to identify characteristic spectroscopic signatures for the presence of multiple excitons of varying order in seeded and non-seeded CdS nanorods. Applying an MCMC sampling approach for global target analysis enables us to determine contributions of multiple exciton decay via Auger recombination and population of surface exciton states to the observed transient dynamics. The influence of surface chemistry, i.e., the nature of the surface ligands on multiexciton dynamics of nanorods is studied.

Semiconductor nanocrystals have gained significant attention due to their tunable optoelectronic properties.[1-3] Besides application as emitters in sensing and imaging,[4, 5] displays[6] or as laser medium[7], in quantum computation and communication[8], nanocrystals have shown potential in light-harvesting applications, i.e. photovoltaics[9] and photocatalysis for solar-to-fuel conversion as a clean source of energy[10]. Special focus has been devoted to heterostructures, e.g. seeded CdS nanorods for their extraordinary light absorption and intrinsic charge separation properties which can be controlled via band-alignment,[11] supporting transfer of charge carriers to a catalytic reaction center and the formation of long-lived charge separation.[12-14] A highly interesting property of semiconductor nanocrystals is the formation of multiexcitons, e.g., via the consecutive absorption of multiple photons or by multiexciton generation (MEG), a process whereby multi-excitons are generated by splitting of a high energy single exciton to two or more low energy excitons.[15, 16] Multiexcitons are of interest for potential applications of nanocrystals in optical amplification[17] and could also be beneficial for charge carrier generation in photovoltaics[18] and for photochemical and photocatalytic processes involving multielectron processes[19, 20]. Unfortunately, the lifetime of multiple excitons is limited through annihilation via Auger recombination, which occurs with rates on the timescale of 10s to 100s of ps in semiconductor nanocrystals.[16, 19, 21] Auger recombination rates have been shown to be tunable via structural parameters as size and shape of nanocrystals, e.g., Auger recombination lifetime scales with volume of the nanocrystal,[22] but also is influenced by the surface area which causes Auger recombination to be faster in CdSe 1D nanorods compared to 0D quantum dots.[16] In heterostructures band alignment and wavefunction engineering impacts Auger recombination lifetimes by controlling the electron hole distributions.[19, 23, 24] Reducing the

overlap between hole and electron wavefunction can suppress Auger recombination. To be able to reliably determine multiexciton lifetimes is crucial to exploit the relations between structure and dynamics for the design particles optimized for a certain application. The standard approach to investigate dynamics involving multiple excitons is to perform transient absorption (TA) spectroscopy measurements with increasing pump intensity observing the decay dynamics of the band-edge bleach feature.[19, 25, 26] The observed additional fast decaying process in band-edge kinetics appearing with increasing pump-intensity are usually assigned to Auger recombination processes and is used to determine the lifetimes of multiple excitons and Auger recombination rate constants. However, the single probe wavelength analysis limited to following bleach decay kinetics could be misleading as the initial fast decaying component can contain not only contributions from bi-excitons, but also higher-order excitonic states depending on the excitation intensity.[22, 27] Klimov and coworkers determined dynamical properties of multiexcitons also of higher order using a subtractive method to extract single exponential dynamics from multi-exponential bleach decay signals.[22] Such results need to be evaluated carefully because the multiexponential behavior in the bleach decay signatures can also arise from population of surface exciton states, i.e. trapping.[22, 28, 29] To facilitate discrimination between multiexciton states of varying order and population of surface states differences in the spectral signatures can be exploited. For this, global analysis of spectrally resolved datasets recorded upon varying excitation intensities needs to be performed to extract besides kinetic information also spectra for the contributing species. Only a few reports exists on efforts to determine besides the dynamical also spectral properties and so far were mainly focused on biexcitons.[30-32] The complexity of the data sets, kinetics for a large number of wavelengths and varying excitation intensities need to be evaluated, presents a challenge for data evaluation. Additionally, TA spectra for the involved

species are broad and expected to strongly overlap with complex line shapes which show for certain species only subtle differences, complicating the evaluation of the quality of the fit and model selection. One approach followed reported relies on standard global analysis of datasets at single pump intensities.[20, 30] Applying this approach the species spectra and decay kinetics for single and biexcitons in CdSe quantum dots have been determined. As the contributing species spectra and rates are expected not to vary with excitation intensity, a simultaneous analysis of varying intensities could improve quality of the time constants and species spectra obtained. This has been realized applying a Markov Chain Monte Carlo (MCMC) sampling approach for global target analysis of transient absorption spectra of $CsPbBr_3$ and CdSe nanocrystals.[31-33] To the best of our knowledge there have been no attempts to analyze spectral and dynamical properties of multiexcitons of higher order applying transient absorption spectroscopy, also considering interferences caused by population of surface exciton states related to the trap states of nanocrystals.

In this work, we are investigating the spectral and dynamic properties of multiexcitons beyond biexcitons in CdSe@CdS and CdS nanorods. To analyze pump intensity dependent spectrally resolved transient absorption data globally over a wide range of pump intensities the MCMC sampling approach for global target analysis was applied.[31] By analyzing the influence of the heterointerface and variations in the surface functionalities influencing surface trap state densities, the role of trapping processes during multiple exciton relaxation is explored.

Results and Discussion

CdSe@CdS nanorods (length 20.0 ± 1.6 nm, width 4.6 ± 0.7 nm) with quasi-type II band alignment (seed size ~2.3 nm) and CdS nanorods (length 21.1 ± 5.3 nm, width 4.1 ± 0.6 nm) capped with trioctylphosphine oxide (TOPO) surface ligands dispersible in toluene were

synthesized following the well-established seeded-growth approach and ligand exchange with mercaptoundecanoic acid (MUA) was performed according to literature reports and the nanorods redispersed in methanol (see Figure S1–S3 for details on sample characterization).[34-36]

Transient absorption spectroscopy was performed spanning the single to multiple excitation regime exciting the sample with pulses with a central wavelength of 400 nm and a pulse duration of 100 fs of varying intensity between 28 and 934 μJ/cm^2. Transient spectra recorded at different excitation intensities at a delay time of 2 ps are depicted for TOPO-capped CdSe@CdS nanorods in toluene in **Figure 2**a. The observed spectral features in the transient spectra are caused by conduction band state filling. The transient absorption spectra show negative features at 464 nm and 566 nm corresponding to a bleach of the lowest excitonic transitions localized in the CdS and the CdSe domains in the seeded nanorods, i.e. the transition between the lowest energy CB electron level $1\sigma_e$ and VB hole level $1\sigma_h$ or $1S_h$ respectively.[19, 37] The population of either of both states leads to bleaches at both excitonic transitions, suggesting that these transitions involve the same CB electron level, indicating type-two band alignment and delocalization of the electron wavefunctions over both domains. The CdS rod bleach signal is more intense than the CdSe seed bleach signal due to the larger volume of the CdS rod shaped shell compared to the CdSe seed. Additionally, at low excitation intensities a photoinduced absorption band is present at 432 nm as shown in Figure 1c. While increasing the pump fluence the intensity of band-edge bleach features increases and broadens, and the photoinduced absorption band disappears, i.e. the positive signature in the spectral region around 432 nm turns into negative signal. Similar spectral change with increasing pump fluence have been observed before for CdSe[30] and CdSe@CdS[38] quantum dots and CdS nanorods[20, 39] and were attributed to a changing initial population of monoexcitons and multiexcitons (given by a Poisson distribution) with increasing pump intensity. After

formation of the monoexciton upon interaction with the probe light a second transition to the lowest excitonic levels is in principle possible but appears at a shifted position with modified transition oscillator strength caused by Coulomb multiparticle interactions in the double excited nanoparticle formed, resulting in negative bleach signatures at the position of the excitonic transitions and the appearance of positive features either red- or blue shifted depending on the type of interaction (binding or repulsive in the generated multiple excited particle).[30, 39, 40] In a biexcitonic state the lowest CB electron level is completely populated and for higher excitonic states also the CB π_e levels are populated additionally. The lowest excitonic transitions are not possible in multiexcitonic states resulting in bleach of the excitonic features and absence of the photoinduced absorption band. Further, caused also by additional bleach contribution from higher excitonic transitions to π_e levels, a broadening of the bleach signatures typically occurs. Hence, the observed disappearance of the photoinduced absorption band and broadening of the bleach signal with increasing excitation intensity is directly associated with the presence of higher order excitons initially generated upon excitation with sufficient intensity. Further, it can be concluded that the temporal development of the TA signal at the position of the photoinduced absorption signal (432 nm) sensitively reports on the decay of multiple excitons. A plot the transient signal at 432 nm in dependence on delay time for varying excitation intensities is presented in **Figure 2**b. At low pump fluences, where only monoexcitons are generated, an immediate positive signal formation is observed upon excitation which slowly decays on the ns timescale. In contrast, at high pump fluences the initial signal after excitation is negative and decays to form a positive signal with increasing delay time. The formation of the photoinduced absorption band takes place on a few 100 ps time scale, which is in the range of Auger recombination times observed in rod shaped semiconductor nanocrystals.[20, 41, 42] Hence this transition from negative to positive signal indicates

the decay of multiexcitons to form monoexcitons, which decay on the ns time scale. Normalized transient spectra at long delay times, show slight differences for low and high excitation intensity. Figure 1c. Taken together with slight differences in the long-term decay dynamics for low and high excitation intensity (Figure 1d), this is first indication that additional states, which might only be accessible via multiexcitons might play a role.

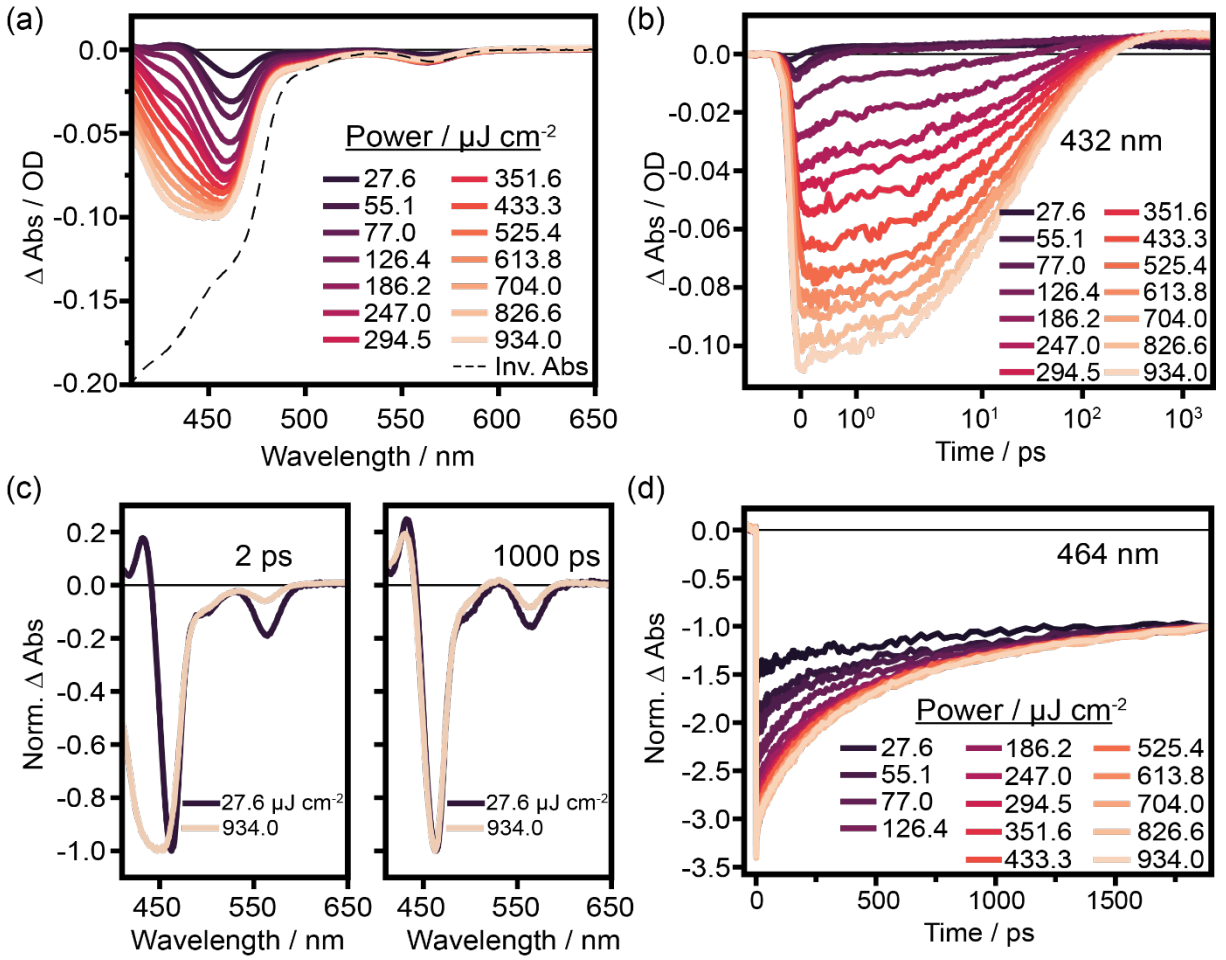

Figure 1. Intensity dependent transient absorption data of TOPO capped CdSe@CdS nanorods excited at 400 nm. (a) Experimental TA spectra at 2 ps after excitation. The dashed black trace shows the inverted steady state absorption spectrum for comparison. (b) Kinetic decay profiles at 432 nm. (c) Normalized transient absorption data at low (black trace) and high intensity (yellow trace) recorded after 2 ps of excitation (left) and ~1000 ps after excitation (right). (d) Transient absorption kinetics at 464 nm with increasing pump intensity normalized at 1900 ps delay time.

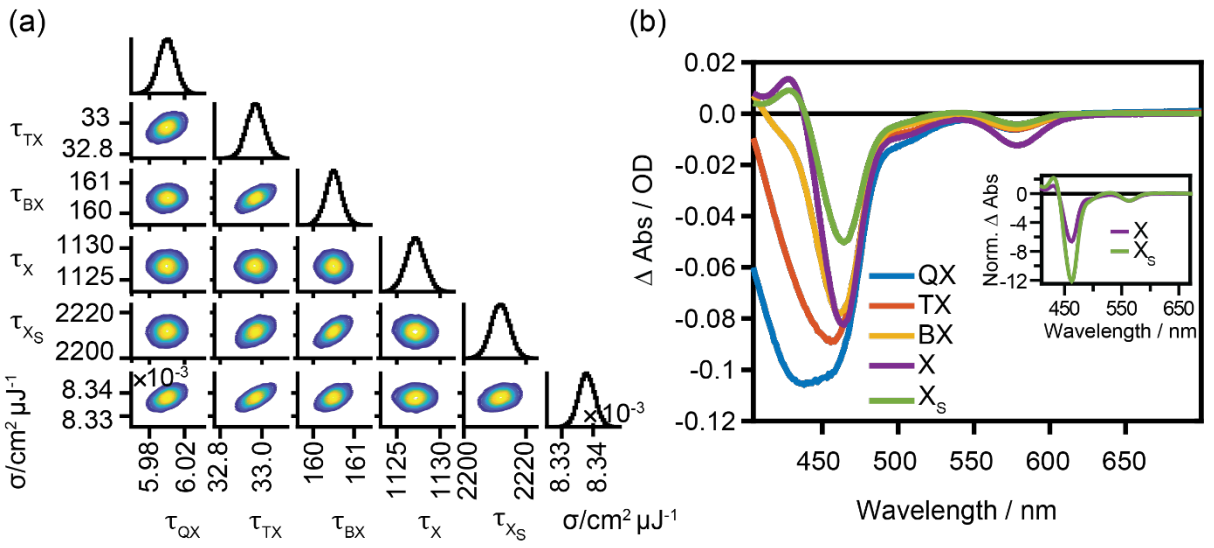

Figure 2. Target model sampling of TOPO capped CdSe@CdS nanorods excited at 400 nm. (a) Corner plot of the posterior probability distribution of the modeled parameters for TOPO-capped CdSe@CdS nanorods determined by MCMC sampling method.[31] The lifetimes are shown in ps. (b) Component spectra of the tetra-exciton (QX, blue trace), tri-exciton (TX, red trace), bi-exciton (BX, orange trace), mono-exciton (X, purple trace), and surface mono-exciton (X_s, green trace) determined by overlaying 100 random samples from the Markov Chain to visually show the deviations among randomly drawn samples. Inset: Component spectra of X and X_s normalized to the lowest CdSe excitonic transition feature.

From these qualitative considerations we can conclude, that in our dataset, increasing initial population of multiexciton states plays a role but we cannot derive any statement on the order of the multiexcitonic states contributing to the data. To retrieve quantitative information on the multiexciton decay, to extract timescales and spectral information on the contributing species, the data needs to be modeled applying a suited kinetic model. The non-radiative annihilation of multiexcitons via Auger recombination occurs according to the established quantized Auger recombination model in a sequential cascade mechanism.[22, 43] This means the initially generated multiexciton of N^{th} order (N being the number of excitons generated and interacting in one particle to form an N^{th} order multiexciton) is annihilated to form $(N-1)^{th}$ order multiexciton, which decays to a $(N-2)^{th}$ order multiexciton and so on until all the multiexcitons have decayed to form monoexciton species. The rate laws for such a scheme can be written as

$$\frac{d[N]}{dt} = -\frac{[N]}{\tau_N}$$
$$\frac{d[N-1]}{dt} = \frac{[N]}{\tau_N} - \frac{[N-1]}{\tau_{N-1}}$$
$$\frac{d[N-2]}{dt} = \frac{[N-1]}{\tau_{N-1}} - \frac{[N-2]}{\tau_{N-2}} \quad (1)$$
$$\dots$$
$$\frac{d[1]}{dt} = \frac{[2]}{\tau_2} - \frac{[1]}{\tau_1}$$

with τ_N being the time constant representing the lifetime of the Nth order multiexcitonic state. The initial population of the multiexcitons in an ensemble of nanorods generated by absorption of light is following a Poisson distribution:

$$P_N(0) = \frac{< N >^N e^{-<N>}}{N!} \quad (2)$$

The average number $< N >$ of excitons per nanorod depends on the excitation intensity and can be estimated from the average energy density (J) and an absorption cross-section scaled with pump power density (σ)

$$< N >= \mathrm{J} \times \sigma \quad (3)$$

Hence, with equation 2 and 3, the excitation intensity dependent initial distribution of population, or in other words, the starting concentrations $c_N(t = 0, J)$ of contributing monoexcitonic and multiexcitonic states of different order is described. With that the transient absorption data can be simulated

$$\Delta\mathrm{A}(\lambda, \mathrm{t}, \mathrm{J}) = \sum_N c_N(t, J) s_N(\lambda) \quad (4)$$

In this approach it is assumed that the component spectra for the contributing species $s_N(\lambda)$ are not changing with time or excitation intensity and that the observed decay kinetic solely is influences by dynamics changing population of the contributing states.

For modeling the excitation intensity dependent dataset for all intensities simultaneously, the parameters to be determined are the time constants for the single annihilation steps in the decay mechanism τ_N, the absorptions cross-section parameter σ, and the component spectra $s_N(\lambda)$ of the species contributing to the transient spectra. This adds up to a large number of unknown variables (order of magnitude 1000) for the whole wavelength and excitation intensity dependent dataset, too many for a standard nonlinear least-squares algorithm. For such problems the Markov Chain Monte Carlo (MCMC) sampling method for target analysis described by Ashner et al. has proven suited to not only to extract time constants and species spectra, but also to deliver measures to evaluate the quality of the model chosen, supporting to identify the correct model to describe the dataset, and derive information on the uncertainty of the determined parameters in form of posterior probability distributions.[31]

We applied this method to analyze the intensity dependent data in the time range 2 to 1000 ps throughout this study. These limits were chosen to focus on contributions from Auger recombination connected population dynamics occurring on the 100s ps time scale. Further, the model assumes a particular spectrum for each contributing species that does not change with time delay or fluence. This affords that hot carrier thermalization, which is connected to a constantly changing spectrum of non-thermalized charge carriers is complete, which is the case after 2 ps.[22, 30, 31]

When applying the simple quantized Auger recombination model to our data, we were unable to describe neither the entire dataset at once (ΔA (λ, t, J), 3D dataset) nor individually fitted intensity

datasets (ΔA (λ, t), 2D datasets). This can be related to our qualitative observation of deviations in the decay kinetics and spectra that at late delay times, which could be an indication of contributions of more than one long-lived species with changing weights depending on the excitation intensity (Figure S4). To account for this, we modified the standard quantized Auger recombination model for multiexciton annihilation by introducing two distinct biexciton decay pathways, one via mono-exciton species (X) with the initial concentration as described by the Poisson distribution and one via an additional species (X_S) formed with no initial concentration but populated during relaxation of higher order excitons (Scheme 1). The splitting parameter ϕ describes the weight of both processes in the multiexciton decay channel. The simplest final kinetic model which was capable to describe our data includes five free species (i.e., tetra-, tri-, bi- and two monoexciton states, X, X_s), splitting parameter ϕ and the free absorption power density scaled cross-section parameter (σ) for optimization.

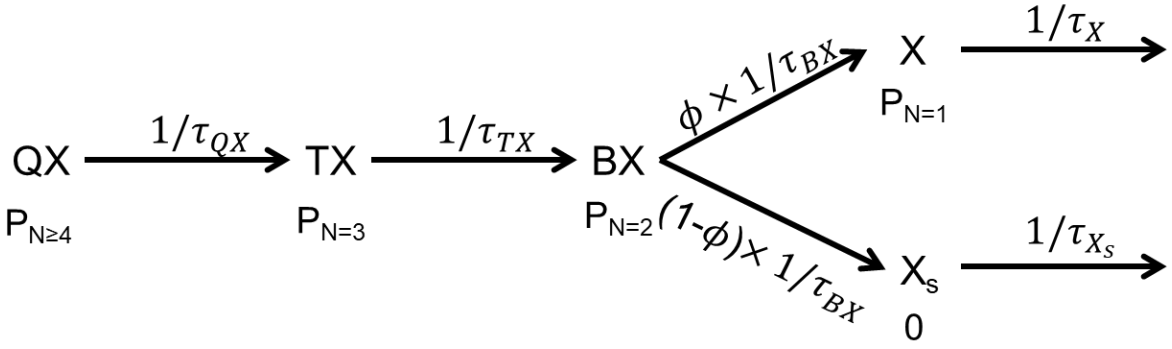

Scheme 1. Modified quantized Auger recombination model applied in target analysis of the intensity dependent transient absorption data in this study: QX, TX, BX, X, X_s stand for tetra-, tri-, bi- and monoexcitons. P_N represents the initial relative concentration of the respective species given by the Poisson distribution. The initial QX population sums over the probability of four or more excitations per nanorod $P(N \geq 4) = 1 - \sum_{N=0}^{N=3} P(N)$. Such higher excitations will have only small contributions due to decay on the sub 1 ps time scale and QX is the highest-order exciton expected to significantly contribute to our dataset.

This modified quantized Auger recombination model describes satisfactorily the experimentally observed dataset in the power density range 77 – 930 μJ/cm2 (see supporting information for

kinetic fits and concentration profiles, Figure S5 and S6.). The maximum likelihood values of the lifetimes and cross-section parameter are summarized in Table 1 and the posterior probability distributions are plotted in **Figure 2**Figure 2a. The splitting parameter ϕ was found to tend to zero in all optimizations performed, i.e., X is only formed directly via initial excitation with a concentration given by the Poisson distribution and all multiexcitons decay via Xs, and in the end $\phi = 0$ was fixed in the model and not optimized. The diagonal plots in the corner plot display the distribution of lifetimes of the five species and the absorption cross-section parameter. The off-diagonal plots show the two-dimensional projections of the posterior probability distribution sampled by the MCMC method illustrating cross-correlations between parameter pairs, which provides an important criterium to evaluate the model especially with respect to overfitting. The round shape of the contour diagrams indicates that the used parameters do not have any needless cross-correlation, i.e., all the parameters are adequately independent of each other, and no redundant parameter is used in the kinetic model. The biexciton lifetime obtained from the fit, ~161 ps, is consistent with that of literature reported Cd based nanorods. [20, 42, 44] The ratio of lifetimes of multiexcitons QX:TX:BX is 0.04:0.20:1, which is very close to the statistical ratio 0.08:0.22:1 predicted for the 1D nanorods.[19, 43] It is important to note that the lifetimes of the long-lived monoexciton species X and X_S are longer than the timeframe modeled, hence the values determined are only estimates with high inaccuracy. The absorption cross-section parameter (σ) found by our model is $8.338 \times 10^{-3}\ cm^2/\mu J$ and corresponds to an absorption cross-section area of $4.14 \times 10^{-15}\ cm^{-2}$, which is close to the literature estimated value of $8.9 \times 10^{-15}\ cm^2$ at 400 nm for similar sized CdSe@CdS nanorods.[37]

In Figure 2b, the species spectra are depicted. Comparing the spectra for the monoexcitonic species to the component spectra of the multiexcitonic species the photoinduced absorption at

432 nm disappears for higher order multiexcitons, in agreement with the discussion above. Further, we observed that the 1σ bleach intensity (λ = 464 nm) ratio in monoexciton (X_S) and biexciton is ~1.6. For a doubly degenerate CdSe quantum dot system, the exciton to biexciton ratio has been shown to be below 2 due to the influence of both Stark effect and state filling effect near the band edge position.[30, 40, 45] For CdSe@CdS nanorods systems we also observed BX/X ratio lower than 2 and further observed that there is almost no increase in 1σ bleach intensity with the formation of higher order excitons.

Comparing the spectra of the two long-lived monoexcitonic species the ratio of the CdS and CdSe bleach features differs significantly. The X_S species shows more intense CdS bleach compared to X (Figure 2b inset). Further, a broad photoinduced absorption band is present in the sub-band gap region above 600 nm in the species spectrum of X_S which is usually assigned to signals from trapped holes.[46-48] This feature is absent in the spectrum of X.

Table 1. Fitted median values and 95% confidence interval of modeled parameters extracted from MCMC Sampling for TOPO-capped CdSe@CdS and CdS and MUA-capped CdSe@CdS nanorods.

Parameter Name	TOPO-capped CdSe@CdS nanorods	MUA-capped CdSe@CdS nanorods	TOPO-capped CdS nanorods
$\tau_{tetraexciton}/ps$	$6.00^{6.02}_{5.98}$	$7.30^{7.31}_{7.28}$	$7.05^{7.07}_{7.04}$
$\tau_{triexciton}/ps$	$32.97^{33.05}_{32.89}$	$37.63^{37.67}_{37.59}$	$30.06^{30.10}_{30.02}$
$\tau_{biexciton}/ps$	$160.5^{160.9}_{160.1}$	$171.7^{171.8}_{171.5}$	$118.1^{118.3}_{117.9}$
$\tau_{monoexciton}/ps$[a]	1127^{1129}_{1125}	1529^{1531}_{1528}	1126^{1128}_{1125}
$\tau_{surface\ exciton}/ps$[a]	2211^{2218}_{2206}	2244^{2246}_{2241}	2996^{3007}_{2985}
Absorption cross-section (σ)/cm^{2}μJ^{-1}	$8.338 \cdot 10^{-3}{}^{8.343 \times 10^{-3}}_{8.333 \times 10^{-3}}$	$7.577 \cdot 10^{-3}{}^{7.589 \times 10^{-3}}_{7.575 \times 10^{-3}}$	$7.650 \cdot 10^{-3}{}^{7.653 \times 10^{-3}}_{7.647 \times 10^{-3}}$

a) the errors given are the modelling uncertainties, but due to the limited delay time window considered, these values are affected by a large experimental additional inaccuracy.

The monoexcitonic state X which is populated upon excitation is the emitting CdSe seed localized state formed in seeded nanorods formed after excitation with 400 nm centered pulses of states mainly localized in the CdS rod part followed by fast hole-localization driven exciton localization (on the few ps timescale).[35, 49] Competing with rod-to-seed localization hole trapping in surface states is possible, the extent depending on the surface ligand.[35] This trapping occurs on the < 2 ps timescale and is not explicitly modeled here. Hence the X state extracted here potentially is a superposition from these two contributions.

The nature of the additional long-lived state is less clear. Here several possibilities need to be considered:

I) The first possibility is a potential trapping in states at the CdSe/CdS interface, which may only be accessible from higher states with a large amount of excess energy, i.e. only accessible form high lying excitonic states or multiexcitonic states. To test on effects connected to the CdSe/CdS interface, we additionally investigated the multiexciton spectral signatures and dynamics of CdS nanorods without CdSe seed to understand the influence of the presence of the CdSe seed on the multiexciton dynamics. Transient absorption spectra of TOPO-capped CdS nanorods recorded at 2 ps after excitation with 100 fs pulses of varying pump intensity from 25–1060 μJ/cm^2 and 400 nm central wavelength are shown in Figure 3. The TA spectra at 2 ps delay time show a negative feature at 453 nm, which can be attributed to the bleach of the lowest excitonic transition, which is in agreement with the absorption spectrum about 10 nm blue shifted compared to the CdSe@CdS nanorods caused by a stronger confinement effect in the CdS nanorods which possess a smaller diameter as the seeded rods (width of CdS@CdS nanorods = 4.6 ± 0.7 nm and width of CdS nanorods = 4.1 ± 0.6 nm). At low pump intensities a positive photoinduced absorption band is present at 413 nm which is disappearing with increasing pump pulse intensity similar to the

observations in seeded nanorods and the spectral signature around 413 nm changes to negative signal. This signature is assigned to a biexciton shifted higher excitonic transition.[39] The pump fluence dependent kinetic traces for CdS nanorods at a probe wavelength of 413 nm are shown in Figure 3b. An immediate formation of the photoinduced absorption band upon excitation with low pump fluences where only mono-excitons are present is observed. In contrast, at high pump fluences when multiexciton formation is to be expected the initial signal after excitation is negative and decays to form a positive signal on a few 100 ps time scale, the typical range for Auger recombination.[22, 43] Hence the general trends observed resemble closely the observations for the seeded nanorods and the transient absorption data is modeled applying the same kinetic model in the MCMC target analysis over the intensity range 96 – 1060 μJ/cm^2 (see Figure S7–S9). The lifetime of higher order excitons (QX and TX) remains unaffected, while the biexciton lifetime in the non-seeded nanorods is reduced to ~118 ps compared to the seeded nanorods, which is reasonably close to the literature reported biexciton lifetime of ~180 ps for slightly longer CdS nanorods.[20] This is presumably due to the removal of quasi type-II band alignment by removal of CdSe seed and thinner CdS nanorod, as the shell thickness is known to influence the biexciton lifetime in core/shell quantum dots.[46] In the component spectra the band-edge bleach of mono-exciton X, biexciton and triexciton is comparable and only slightly increases with tetra-exciton formation. The photoinduced absorption feature is only present in the monoexcitonic species and disappears for the multiexcitons similar to CdSe@CdS nanorods. Furthermore, only X_S shows the positive photoinduced sub bandgap feature in line with our observation for CdSe@CdS seeded nanorods. To summarize, also for the CdS nanorods a second long-lived species is present which shows similar spectral distinction compared to X. From this we can conclude that the appearance of this species is not related to the presence of the CdSe/CdS interface.

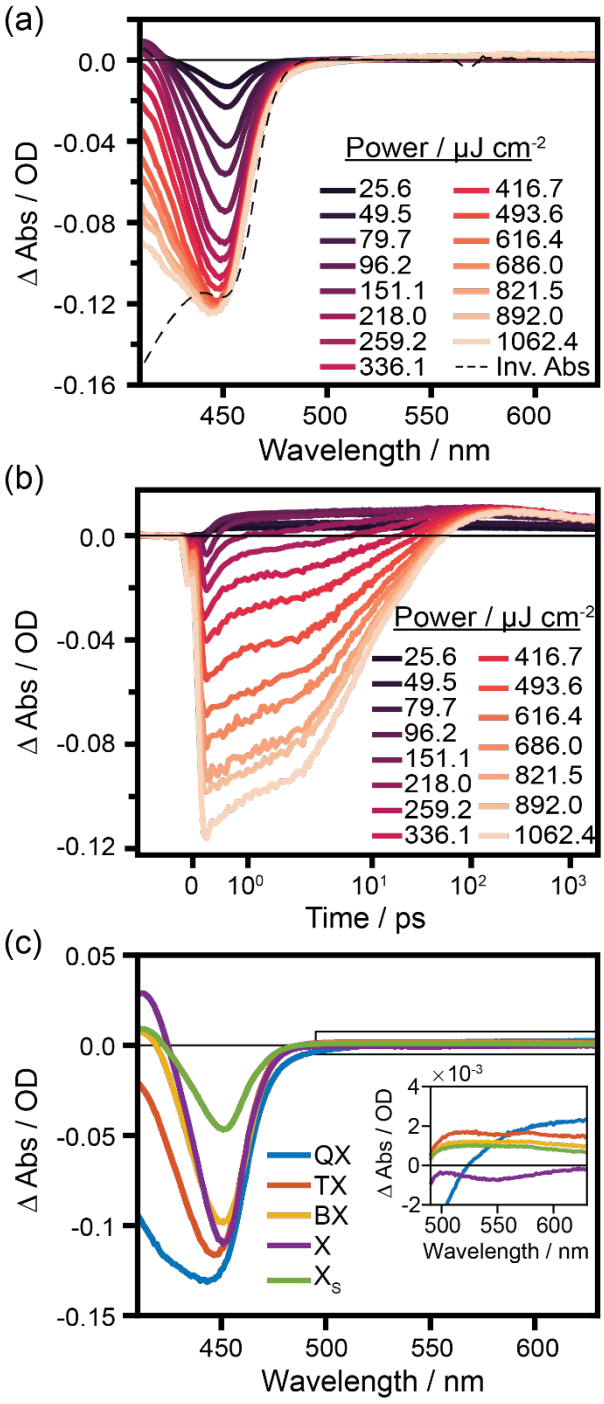

Figure 3. (a) Intensity dependent transient absorption (TA) spectra of TOPO-capped CdS nanorods excited with 400 nm pump pulse at 2 ps after excitation and inverted absorption spectrum for comparison. (b) Kinetic traces at 413 nm probe wavelength. (c) Modeled component spectra of CdS nanorods capped with TOPO plotted by drawing 100 random samples from the Markov Chain and overlaid on top of each other with same color, to show the deviations among different

samples. Insets show the respective zoomed in spectra of sub band-edge photoinduced absorption band.

II) A second possibility is the origin of the X_S state to be related to trapping and localization of excitons at surface sites, hence formation of surface exciton states, which only can be populated from states with sufficient amount of excess energy, e.g., hot multiexcitons and hot monoexcitons appearing during the cascade like multiexciton annihilation process.[17, 28] Though dissipation of excess energy is fast, barrierless population of trap states which are not accessible from the lowest band edge monoexcitonic states can occur efficiently from these states.[50, 51] The exact nature of such surface excitons is not fully revealed yet, but contributions from both hole and electron trapping are discussed.[50, 51] Comparing the spectral shape of the two monoexcitonic species supports this claim of a surface excitonic species X_S. The different relative contributions of CdSe and CdS domains in these mono-exciton species are in agreement with an X_S species related to the surface states showing stronger CdS bleach contributions due to localization in the CdS domain at the surface of the nanorods. One alternative explanation could relate X_S to the formation of charged mono-excitons (trions).[52, 53] However, the reported lifetimes of a charged trion in these type of nanorods is <<1 ns.[52] The lifetime of X and X_S species observed in our experiment are (though the values determined are of limited accuracy due to the limited time window of delay times evaluated) significantly longer. To check on the influence of surface chemistry, CdSe@CdS nanorods with the original TOPO ligand being exchanged by MUA ligands were investigated. Changing the surface ligands modifies the surface chemistry and hence the density of available hole and electron trap states.[35] The MUA-capped nanorods show similar spectral features and dynamic behavior as observed for TOPO-capped CdSe@CdS nanorods. Applying the kinetic model described above the fitted parameters, i.e. the lifetimes and species spectra, differ only marginally (Table 1). The modeled results for MUA functionalized nanorods are given in supporting information (Figure

S10–S12). Interestingly, after ligand exchange the band-edge bleach intensities of all modeled excitons remain similar and do not follow the intensity increase trend as observed in case of TOPO-capped nanorods. The species associated spectrum of X_S shows a similar 40% band-edge bleach reduction compared to species X as observed in case of native nanorods. To directly compare the influence of ligand exchange on the spectra of each excitonic species of TOPO and MUA capped nanorods, we normalized the modeled species spectra datasets of TOPO and MUA capped nanorods to their maximum bleach, i.e., to respective tetra-exciton bleach (Figure 4). This allows for a direct comparison of the spectral shapes of the respective species in dependence of the surface ligand. The normalized spectra (Figure 4) show that the CdS bleach intensity of the other higher order and mono-excitons increases after ligand exchange with MUA. The X_S traces show increased PA after the ligand exchange which might indicate increased hole trapping contributions in the MUA capped nanorods, which supports surface exciton related state. A final aspect to consider is the possibility that surface trap states can also appear during the measurement by illumination induced changes in the surface chemistry by ligand dissociation[54, 55] and lattice distortions[56] and hence influence the formation of surface localized excitons by reversible and non-reversible effects. A comparison with datasets of pre-illuminated TOPO-capped nanorods shows qualitatively and quantitatively similar behavior with increasing pump pulse intensity compared to non-illuminated samples (see supporting information S13-S23). This indicates that either, illumination induced changes are not playing a role, or are appearing very fast during the first few scans during the measurements.

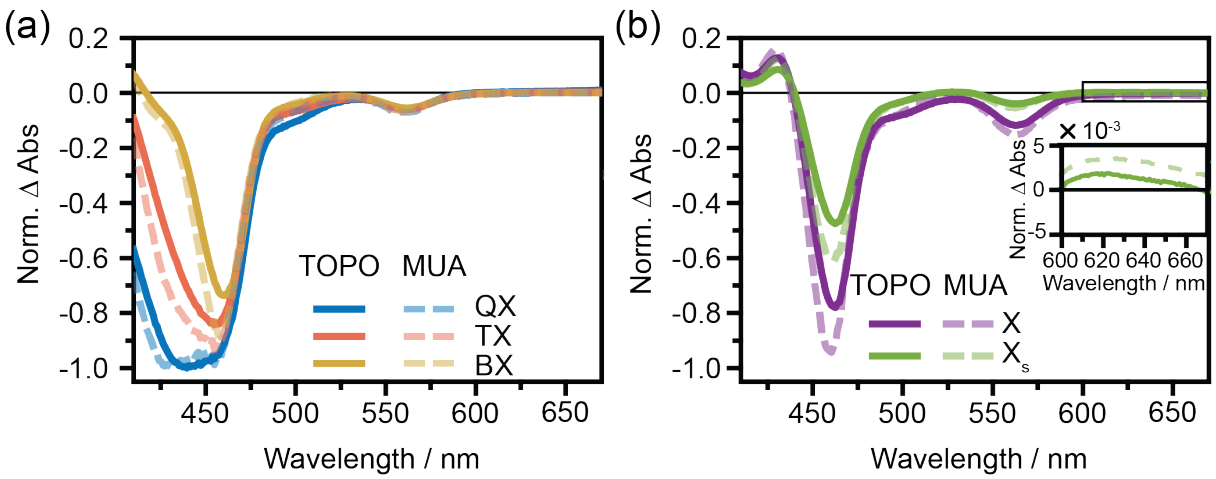

Figure 4. (a) Multiexciton component spectra of TOPO-capped (dark traces) and MUA-capped (light traces). (b) Monoexciton component spectra of TOPO-capped (dark traces) and MUA-capped (light traces) nanorods. Insets: sub band-edge photoinduced absorption band. The datasets are normalized to the maximum bleach signature of the tetraexciton for comparison.

Conclusions

In this work we investigated spectral and dynamical properties of multiexcitons CdSe@CdS seeded nanorods. By evaluating excitation-intensity dependent transient absorption data applying an MCMC sampling method for target analysis we are able to extract species spectra up to tetra-excitons. Further, we show that the holistic view of entire intensity dependent transient absorption can help us to detect the decay pathways via surface excitons, which is hard to account during analyzing single wavelength kinetics or single power transient absorption data and potentially helps to distinguish the fast decay dynamics shown by multiexciton and surface excitons.

Materials and Methods

All the chemicals and solvent used in the synthesis of CdSe@CdS nanorods and CdS nanorods were purchased from Sigma Aldrich (Merck KGaA, Darmstadt, Germany) except for octadecyl phosphonic acid (ODPA) which was purchased from Carl Roth GmbH + Co. KG (Karlsruhe,

Germany) and used without further purification. The solvents toluene and methanol used were dry and deoxygenated and of spectroscopic grade.

CdSe@CdS[36] and CdS[20] nanorods were prepared using a seeded-growth approach and the original TOPO ligands exchanged with MUA ligands following established protocols.[35] For a detailed description see supporting information.

The femtosecond-TA data was recorded using a home built transient absorption setup with a detection system from Pascher Instruments AB. A regenerative Ti:sapphire amplifier (Astrella, Coherent, USA) delivering pulses centered at 800 nm with ~100 fs full width at half maxima, 5 mJ pulse energy, and 1 kHz pulse repetition rate. The output fundamental is split into several beams. One part is travelling over a 2 ns delay line and is focused onto a rotating CaF_2 window to generate broadband white light continuum (300 – 700 nm). The continuum is split into probe, which is focused on the sample and a reference beam. To generate the excitation pulses 2 mJ of the fundamental output of the amplifier pumping an optical parametric amplifier (TOPAS, Light conversion, Lithuania) to produce tunable pump pulses. For our experiments pump pulses with central wavelength of 400 nm were generated. The relative polarization of pump and probe is set to magic angle 54,7°. A mechanical chopper reduces the repetition rate of the pump pulses to 500 Hz and the pump is focused to the sample (beam diameter 400 μm). The spectra of probe and reference pulses are recorded by CCD array detectors after passing a Czerny-Turner spectrograph with 150 mm focal length (SP2150, Princeton Instruments). The obtained TA data was chirp corrected using a python-based package KiMoPack.[57] The intensity dependent TA data in time range 2 – 1000 ps were fit using a slightly modified script published for target model sampling using Markov Chain Monte Carlo method.[16] The script was modified to adapt our target model described in main text.

ASSOCIATED CONTENT

Supporting Information. The following files are available free of charge. Experimental details on nanoparticle synthesis, steady state absorption and photoluminescence spectra, TEM images, MCMC fits and concentration profiles.

AUTHOR INFORMATION

Corresponding Author

Krishan Kumar - Department Functional Interfaces, Leibniz Institute of Photonic Technology Jena, Albert-Einstein-Straße 9, 07745 Jena, Germany

Email: kumar.krishan@leibniz-ipht.de

Maria Wächtler - Chemistry Department and State Research Center OPTIMAS, RPTU Kaiserslautern-Landau, Erwin-Schrödinger-Str. 52, 67663 Kaiserslautern, Germany

Email: maria.waechtler@chem.rptu.de

Author Contributions

The manuscript was written through contributions of all authors. KK: Conceptualization, Methodology, Data analysis, Writing - original draft. MW: Conceptualization, Resources, Investigation, Supervision, Funding acquisition, Writing - original draft. All authors have given approval to the final version of the manuscript.

Funding Sources

German Research Foundation (DFG), project number 468735112 – KU 4220/1-1 and project number 364549901–TRR234 CATALIGHT, TP B04.

Notes

The authors declare no competing financial interest.

ACKNOWLEDGMENT

We thank the German Research Foundation (DFG) for supporting this work under the project number 364549901–TRR234 CATALIGHT, TP B04 and project number 468735112 – KU 4220/1-1. We thank Jan Dellith and Andrea Dellith for acquiring TEM images. We gratefully acknowledge discussions with Mathias Micheel and Raktim Baruah. KK is thankful to Tara Chand for fruitful discussions on the modeling routine.

REFERENCES

1. Talapin, D. V.; Lee, J. S.; Kovalenko, M. V.; Shevchenko, E. V., Prospects of Colloidal Nanocrystals for Electronic and Optoelectronic Applications. *Chem. Rev.* **2010,** *110* (1), 389-458.
2. García de Arquer, F. P.; Talapin, D. V.; Klimov, V. I.; Arakawa, Y.; Bayer, M.; Sargent, E. H., Semiconductor quantum dots: Technological progress and future challenges. *Science* **2021,** *373* (6555), eaaz8541.
3. Smith, A. M.; Nie, S., Semiconductor Nanocrystals: Structure, Properties, and Band Gap Engineering. *Accounts. Chem. Res.* **2010,** *43* (2), 190-200.
4. Zhou, J.; Liu, Y.; Tang, J.; Tang, W., Surface ligands engineering of semiconductor quantum dots for chemosensory and biological applications. *Materials Today* **2017,** *20* (7), 360-376.
5. Silvi, S.; Credi, A., Luminescent sensors based on quantum dot–molecule conjugates. *Chem. Soc. Rev.* **2015,** *44* (13), 4275-4289.
6. Panfil, Y. E.; Oded, M.; Banin, U., Colloidal Quantum Nanostructures: Emerging Materials for Display Applications. *Angewandte Chemie International Edition* **2018,** *57* (16), 4274-4295.
7. Park, Y.-S.; Roh, J.; Diroll, B. T.; Schaller, R. D.; Klimov, V. I., Colloidal quantum dot lasers. *Nature Reviews Materials* **2021,** *6* (5), 382-401.
8. Kagan, C. R.; Bassett, L. C.; Murray, C. B.; Thompson, S. M., Colloidal Quantum Dots as Platforms for Quantum Information Science. *Chem. Rev.* **2021,** *121* (5), 3186-3233.
9. Kirmani, A. R.; Luther, J. M.; Abolhasani, M.; Amassian, A., Colloidal Quantum Dot Photovoltaics: Current Progress and Path to Gigawatt Scale Enabled by Smart Manufacturing. *ACS Energy Letters* **2020,** *5* (9), 3069-3100.
10. Wu, K.; Lian, T., Quantum confined colloidal nanorod heterostructures for solar-to-fuel conversion. *Chem. Soc. Rev.* **2016,** *45* (14), 3781-3810.

11. Sitt, A.; Hadar, I.; Banin, U., Band-gap engineering, optoelectronic properties and applications of colloidal heterostructured semiconductor nanorods. *Nano Today* **2013,** *8* (5), 494-513.
12. Wu, K. F.; Zhu, H. M.; Lian, T. Q., Ultrafast Exciton Dynamics and Light-Driven H-2 Evolution in Colloidal Semiconductor Nanorods and Pt-Tipped Nanorods. *Accounts. Chem. Res.* **2015,** *48* (3), 851-859.
13. Wächtler, M.; Kalisman, P.; Amirav, L., Charge-Transfer Dynamics in Nanorod Photocatalysts with Bimetallic Metal Tips. *J. Phys. Chem. C* **2016,** *120*, 24491-24497.
14. Moroz, P.; Boddy, A.; Zamkov, M., Challenges and Prospects of Photocatalytic Applications Utilizing Semiconductor Nanocrystals. *Frontiers in Chemistry* **2018,** *6*.
15. Beard, M. C., Multiple Exciton Generation in Semiconductor Quantum Dots. *The Journal of Physical Chemistry Letters* **2011,** *2* (11), 1282-1288.
16. Klimov, V. I., Mechanisms for Photogeneration and Recombination of Multiexcitons in Semiconductor Nanocrystals: Implications for Lasing and Solar Energy Conversion. *The Journal of Physical Chemistry B* **2006,** *110* (34), 16827-16845.
17. Ahn, N.; Livache, C.; Pinchetti, V.; Klimov, V. I., Colloidal Semiconductor Nanocrystal Lasers and Laser Diodes. *Chem. Rev.* **2023,** *123* (13), 8251-8296.
18. Beard, M. C.; Luther, J. M.; Semonin, O. E.; Nozik, A. J., Third Generation Photovoltaics based on Multiple Exciton Generation in Quantum Confined Semiconductors. *Accounts. Chem. Res.* **2013,** *46* (6), 1252-1260.
19. Zhu, H.; Yang, Y.; Lian, T., Multiexciton Annihilation and Dissociation in Quantum Confined Semiconductor Nanocrystals. *Accounts. Chem. Res.* **2013,** *46* (6), 1270-1279.
20. Ben-Shahar, Y.; Philbin, J. P.; Scotognella, F.; Ganzer, L.; Cerullo, G.; Rabani, E.; Banin, U., Charge Carrier Dynamics in Photocatalytic Hybrid Semiconductor–Metal Nanorods: Crossover from Auger Recombination to Charge Transfer. *Nano Lett* **2018,** *18* (8), 5211-5216.
21. Melnychuk, C.; Guyot-Sionnest, P., Multicarrier Dynamics in Quantum Dots. *Chem. Rev.* **2021,** *121* (4), 2325-2372.
22. Klimov, V. I.; Mikhailovsky, A. A.; McBranch, D. W.; Leatherdale, C. A.; Bawendi, M. G., Quantization of Multiparticle Auger Rates in Semiconductor Quantum Dots. *Science* **2000,** *287* (5455), 1011-1013.
23. García-Santamaría, F.; Chen, Y.; Vela, J.; Schaller, R. D.; Hollingsworth, J. A.; Klimov, V. I., Suppressed Auger Recombination in "Giant" Nanocrystals Boosts Optical Gain Performance. *Nano Lett* **2009,** *9* (10), 3482-3488.
24. Kong, D.; Jia, Y.; Ren, Y.; Xie, Z.; Wu, K.; Lian, T., Shell-Thickness-Dependent Biexciton Lifetime in Type I and Quasi-Type II CdSe@CdS Core/Shell Quantum Dots. *J. Phys. Chem. C* **2018,** *122* (25), 14091-14098.
25. Klimov, V. I., Spectral and Dynamical Properties of Multiexcitons in Semiconductor Nanocrystals. *Annu. Rev. Phys. Chem.* **2007,** *58* (1), 635-673.
26. Kumar, K.; Wächtler, M., Unravelling Dynamics Involving Multiple Charge Carriers in Semiconductor Nanocrystals. *Nanomaterials* **2023,** *13* (9), 1579.
27. Strandell, D. P.; Ghosh, A.; Zenatti, D.; Nagpal, P.; Kambhampati, P., Direct Observation of Higher Multiexciton Formation and Annihilation in CdSe Quantum Dots. *The Journal of Physical Chemistry Letters* **2023,** *14* (30), 6904-6911.
28. Tyagi, P.; Kambhampati, P., False multiple exciton recombination and multiple exciton generation signals in semiconductor quantum dots arise from surface charge trapping. *J. Chem. Phys.* **2011,** *134* (9), 094706.

29. Malko, A. V.; Mikhailovsky, A. A.; Petruska, M. A.; Hollingsworth, J. A.; Klimov, V. I., Interplay between Optical Gain and Photoinduced Absorption in CdSe Nanocrystals. *The Journal of Physical Chemistry B* **2004,** *108* (17), 5250-5255.
30. Labrador, T.; Dukovic, G., Simultaneous Determination of Spectral Signatures and Decay Kinetics of Excited State Species in Semiconductor Nanocrystals Probed by Transient Absorption Spectroscopy. *J. Phys. Chem. C* **2020,** *124* (15), 8439-8447.
31. Ashner, M. N.; Winslow, S. W.; Swan, J. W.; Tisdale, W. A., Markov Chain Monte Carlo Sampling for Target Analysis of Transient Absorption Spectra. *J. Phys. Chem. A* **2019,** *123* (17), 3893-3902.
32. Shulenberger, K. E.; Sherman, S. J.; Jilek, M. R.; Keller, H. R.; Pellows, L. M.; Dukovic, G., Exciton and biexciton transient absorption spectra of CdSe quantum dots with varying diameters. *J. Chem. Phys.* **2024,** *160* (1).
33. Ashner, M. N.; Shulenberger, K. E.; Krieg, F.; Powers, E. R.; Kovalenko, M. V.; Bawendi, M. G.; Tisdale, W. A., Size-Dependent Biexciton Spectrum in CsPbBr3 Perovskite Nanocrystals. *ACS Energy Letters* **2019,** *4* (11), 2639-2645.
34. Talapin, D. V.; Nelson, J. H.; Shevchenko, E. V.; Aloni, S.; Sadtler, B.; Alivisatos, A. P., Seeded Growth of Highly Luminescent CdSe/CdS Nanoheterostructures with Rod and Tetrapod Morphologies. *Nano Lett* **2007,** *7* (10), 2951-2959.
35. Micheel, M.; Liu, B.; Wächtler, M., Influence of Surface Ligands on Charge-Carrier Trapping and Relaxation in Water-Soluble CdSe@CdS Nanorods. *Catalysts* **2020,** *10* (10), 1143.
36. Amirav, L.; Alivisatos, A. P., Photocatalytic Hydrogen Production with Tunable Nanorod Heterostructures. *J. Phys. Chem. Lett.* **2010,** *1* (7), 1051-1054.
37. Wu, K. F.; Rodriguez-Cordoba, W. E.; Liu, Z.; Zhu, H. M.; Lian, T. Q., Beyond Band Alignment: Hole Localization Driven Formation of Three Spatially Separated Long-Lived Exciton States in CdSe/CdS Nanorods. *Acs Nano* **2013,** *7* (8), 7173-7185.
38. Zhu, H.; Song, N.; Rodríguez-Córdoba, W.; Lian, T., Wave Function Engineering for Efficient Extraction of up to Nineteen Electrons from One CdSe/CdS Quasi-Type II Quantum Dot. *J. Am. Chem. Soc.* **2012,** *134* (9), 4250-4257.
39. Liu, Y.; Cullen, D. A.; Lian, T., Slow Auger Recombination of Trapped Excitons Enables Efficient Multiple Electron Transfer in CdS–Pt Nanorod Heterostructures. *J. Am. Chem. Soc.* **2021,** *143* (48), 20264-20273.
40. Klimov, V. I., Optical Nonlinearities and Ultrafast Carrier Dynamics in Semiconductor Nanocrystals. *The Journal of Physical Chemistry B* **2000,** *104* (26), 6112-6123.
41. Taguchi, S.; Saruyama, M.; Teranishi, T.; Kanemitsu, Y., Quantized Auger recombination of biexcitons in CdSe nanorods studied by time-resolved photoluminescence and transient-absorption spectroscopy. *Phys. Rev. B* **2011,** *83* (15), 155324.
42. Htoon, H.; Hollingsworth, J. A.; Dickerson, R.; Klimov, V. I., Effect of Zero- to One-Dimensional Transformation on Multiparticle Auger Recombination in Semiconductor Quantum Rods. *Phys. Rev. Lett.* **2003,** *91* (22), 227401.
43. Klimov, V. I.; McGuire, J. A.; Schaller, R. D.; Rupasov, V. I., Scaling of multiexciton lifetimes in semiconductor nanocrystals. *Phys. Rev. B* **2008,** *77* (19), 195324.
44. Zhu, H.; Lian, T., Enhanced Multiple Exciton Dissociation from CdSe Quantum Rods: The Effect of Nanocrystal Shape. *J. Am. Chem. Soc.* **2012,** *134* (27), 11289-11297.
45. Ghosh, T.; Dehnel, J.; Fabian, M.; Lifshitz, E.; Baer, R.; Ruhman, S., Spin Blockades to Relaxation of Hot Multiexcitons in Nanocrystals. *The Journal of Physical Chemistry Letters* **2019,** *10* (10), 2341-2348.

46. Grennell, A. N.; Utterback, J. K.; Pearce, O. M.; Wilker, M. B.; Dukovic, G., Relationships between Exciton Dissociation and Slow Recombination within ZnSe/CdS and CdSe/CdS Dot-in-Rod Heterostructures. *Nano Lett* **2017,** *17* (6), 3764-3774.
47. Utterback, J. K.; Ruzicka, J. L.; Hamby, H.; Eaves, J. D.; Dukovic, G., Temperature-Dependent Transient Absorption Spectroscopy Elucidates Trapped-Hole Dynamics in CdS and CdSe Nanorods. *The Journal of Physical Chemistry Letters* **2019,** *10* (11), 2782-2787.
48. Jasrasaria, D.; Philbin, J. P.; Yan, C.; Weinberg, D.; Alivisatos, A. P.; Rabani, E., Sub-Bandgap Photoinduced Transient Absorption Features in CdSe Nanostructures: The Role of Trapped Holes. *J. Phys. Chem. C* **2020,** *124* (31), 17372-17378.
49. Wu, K.; Hill, L. J.; Chen, J.; McBride, J. R.; Pavlopolous, N. G.; Richey, N. E.; Pyun, J.; Lian, T., Universal Length Dependence of Rod-to-Seed Exciton Localization Efficiency in Type I and Quasi-Type II CdSe@CdS Nanorods. *ACS Nano* **2015,** *9* (4), 4591-4599.
50. Saari, J. I.; Dias, E. A.; Reifsnyder, D.; Krause, M. M.; Walsh, B. R.; Murray, C. B.; Kambhampati, P., Ultrafast Electron Trapping at the Surface of Semiconductor Nanocrystals: Excitonic and Biexcitonic Processes. *The Journal of Physical Chemistry B* **2013,** *117* (16), 4412-4421.
51. Lenngren, N.; Abdellah, M. A.; Zheng, K.; Al-Marri, M. J.; Zigmantas, D.; Žídek, K.; Pullerits, T., Hot electron and hole dynamics in thiol-capped CdSe quantum dots revealed by 2D electronic spectroscopy. *Phys. Chem. Chem. Phys.* **2016,** *18* (37), 26199-26204.
52. Wang, J.; Ding, T.; Wu, K., Coulomb Barrier for Sequential Two-Electron Transfer in a Nanoengineered Photocatalyst. *J. Am. Chem. Soc.* **2020,** *142* (32), 13934-13940.
53. Park, Y.-S.; Bae, W. K.; Pietryga, J. M.; Klimov, V. I., Auger Recombination of Biexcitons and Negative and Positive Trions in Individual Quantum Dots. *ACS Nano* **2014,** *8* (7), 7288-7296.
54. Shulenberger, K. E.; Keller, H. R.; Pellows, L. M.; Brown, N. L.; Dukovic, G., Photocharging of Colloidal CdS Nanocrystals. *J. Phys. Chem. C* **2021,** *125* (41), 22650-22659.
55. Harvey, S. M.; Olshansky, J. H.; Li, A.; Panuganti, S.; Kanatzidis, M. G.; Hupp, J. T.; Wasielewski, M. R.; Schaller, R. D., Ligand Desorption and Fragmentation in Oleate-Capped CdSe Nanocrystals under High-Intensity Photoexcitation. *J. Am. Chem. Soc.* **2024,** *146* (6), 3732-3741.
56. Guzelturk, B.; Cotts, B. L.; Jasrasaria, D.; Philbin, J. P.; Hanifi, D. A.; Koscher, B. A.; Balan, A. D.; Curling, E.; Zajac, M.; Park, S.; Yazdani, N.; Nyby, C.; Kamysbayev, V.; Fischer, S.; Nett, Z.; Shen, X.; Kozina, M. E.; Lin, M.-F.; Reid, A. H.; Weathersby, S. P.; Schaller, R. D.; Wood, V.; Wang, X.; Dionne, J. A.; Talapin, D. V.; Alivisatos, A. P.; Salleo, A.; Rabani, E.; Lindenberg, A. M., Dynamic lattice distortions driven by surface trapping in semiconductor nanocrystals. *Nature Communications* **2021,** *12* (1), 1860.
57. Müller, C.; Pascher, T.; Eriksson, A.; Chabera, P.; Uhlig, J., KiMoPack: A python Package for Kinetic Modeling of the Chemical Mechanism. *J. Phys. Chem. A* **2022,** *126* (25), 4087-4099.

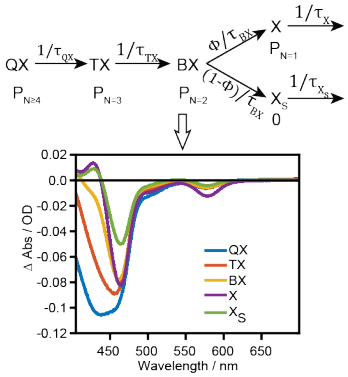

TOC figure